Mechatronics 51 (2018) 8–18

Contents lists available at ScienceDirect

Mechatronics

journal homepage: www.elsevier.com/locate/mechatronics

Design of a Series Elastic Transmission for hand exoskeletons☆

M. Bianchi*,[a], M. Cempini[b], R. Conti[a], E. Meli[a], A. Ridolfi[a], N. Vitiello[b,c], B. Allotta[a,c]

[a] Department of Industrial Engineering (DIEF), University of Florence, Via di Santa Marta 3, Florence 50139, Italy
[b] The BioRobotics Institute, Scuola Superiore Sant'Anna, Viale Rinaldo Piaggio 34, Pontedera 56025, PI, Italy
[c] Fondazione Don Carlo Gnocchi, Florence, Italy

ARTICLE INFO

Keywords:
Portable robotics
Wearable robotics
Hand exoskeleton
Hand disabilities
Series Elastic Actuator
Topology optimization

ABSTRACT

Recently, the wearable robotic field has become extremely prolific in terms of active devices for human body assistance. Nevertheless, unfortunately, owing to strictly motor and sensor requirements in terms of mechanism, weight, size and dexterous manipulation capabilities, portable hand exoskeletons for rehabilitation and assistance have not been developed as much as the exoskeletons for lower and upper limbs; in fact, only a few of them present an outcome of their use in the clinical practice as positive as expected.

This research work aims at designing an aid for the hand function based on exoskeleton technologies for patients who have lost or injured their hand skills.

In particular, this paper presents a novel Series Elastic Transmission (SET) used as power transmission on a Hand Exoskeleton System (HES) based on a Series Elastic Actuator (SEA). The elastic element of the transmission has been designed through the innovative topology optimization approach which has led to manufacture a component whose mechanical features strictly replicate the desired ones. The authors have validated the proposed approach by testing a real elastic component. Suitable mechanical tests, whose results are reported in the paper, were executed in order to evaluate the goodness of the design procedure.

1. Introduction

The demand for rehabilitation therapy has been increasing rapidly in the last years. Two aspects are contributing significantly to this situation. The former is that aging is a global problem, so the number of elderly people, who need resources for rehabilitative therapy, is going to raise unceasingly. The latter is that, not only as a consequence of aging, more people are suffering from neurological and musculoskeletal diseases such as stroke [1], Parkinson's Disease [2] and degenerative arthritis [3].

From the rehabilitation viewpoint, successful sessions require to perform intense and continuous therapeutic tasks. In this field, robotic systems allow to provide prolonged and high-intensity rehabilitation treatments, involving a reduction of costs and burden for the therapists. Wearable robotic devices are indeed strongly addressed by rehabilitation researches [4], because they can control and manage independently the user's single body segments and anatomical motions or joints.

Unfortunately, up to 66% of post-stroke patients cannot regain the dexterity of the damaged arm after 6 months from the stroke [5,6]. In some cases, hand functions may not be totally reacquired even after an intense rehabilitation process. Thus, the hand exoskeletons may serve as an aid to assist the user in the Activities of Daily Living (ADLs) amplifying the hand gripping force or automating the motion.

Even if robotic technologies are more and more pervasive and deployed in clinical environments, reliability and cost-effectiveness are still mandatory aspects for their acceptance and use during the ADLs. These tools need to have flexibility to meet various sets of requirements and also societal expectations. Novel methods and tools need also to be adaptable, to be used by different patients and with different kinds of settings. New solutions should be easy to use and they should be accepted by end-users: elderly/patients, medics, care service providers but also insurance companies and such.

For all these reasons, the adaptability of a robotic device fulfills a key role in the development of human-interactive machines [7,8]. In this regard, rising research activities on rehabilitation and assistive robotics are focusing on these technological advancements [9]. In particular, many researches struggle with reaching the conflictive requirements imposed by such devices: both high precision of motion and of exchanged interaction forces, and inherent safety and adaptability [10] are requested.

Soft systems have been widely investigated in this scenario and both

☆ This paper was recommended for publication by Associate Editor Dr. Lorenzo Masia.

* Corresponding author.
E-mail addresses: matteo.bianchi@unifi.it (M. Bianchi), a.ridolfi@unifi.it (A. Ridolfi).

https://doi.org/10.1016/j.mechatronics.2018.02.010
Received 9 July 2017; Received in revised form 16 October 2017; Accepted 21 February 2018
Available online 08 March 2018
0957-4158/

pneumatic [11,12] and tendon-driven [13–15] gloves represent nowadays valid solutions in the wearable robotics field.

Many strategies have been studied and also adopted to achieve a suitable compliance even in rigid active robots: inherent compliance obtained through compliant actuators [16], deformable structures [17], smart materials [18,19] or emulated compliance obtained through impedance or admittance controller [20]. However, even if they represent a very promising solution, when highly dependable and robust systems are needed, classic actuation technologies (electrical motors or hydraulic pistons) are preferred, because of easy control and high reliability yielded by their wide use in different applications. In these cases, compliance can be embedded within the transmission.

According to this, several scientific and technologies solutions are reported in literature [21,22]. Among them, one of the most promising is the well-known Series-Elastic Actuators (SEAs, [23]) technology. Such design provides a pre-defined mechanical stiffness, properly combined with suitable sensors, interposed in the mechanical power flux pathway. This solution allows to measure the forces exchanged between the mechatronic system and the external environment, storing an energy load during the interaction, and also providing the safety of not fasten the person to a rigid robot [21].

SEA architectures are currently adopted in wearable robotics by many devices, e.g. exoskeletons [24–27]; most of them usually proposes specific and properly designed custom springs or elastic mechanical assemblies to realize revolute actuated joints, coupled with the hip, knee, shoulder or elbow joints of the wearer.

As reported above, the SEA approach lowers the rigidity of the robotic structure but its use has a negative effect on the performance of the actuated joint, limiting the bandwidth to its natural frequency and the maximum output force to a trade-off with the maximum strain of the compliant element. Thus, the design of a SEA faces the hurdle in matching the maximum bearable deformation and the specific stiffness, according to the desired performances, into the small given required space. Up to now, results from the state of the art are still under investigation to be easily implemented in real applications, especially concerning the exoskeletons field.

Exoskeletons for the human hand and their actuation technologies represent a very prolific topic [28] and many devices have been presented in literature [29–31]. Nevertheless, the state of the art shows that it is very hard to achieve a SEA architecture in this case, because of lack of physical room and compatibility with the hand morphology. Nonetheless, the interest in force-controllable hand exoskeletons is high, not only for rehabilitation treatment, but also for haptics or teleoperation [32].

The aim of the presented work is the design of a novel Series Elastic Transmission (SET) developed to be exploited on hand exoskeletons.

In this study, particularly, the proposed SET has been designed to be integrated in the Hand Exoskeleton System (HES) developed by the Department of Industrial Engineering of the University of Florence [33]. The fully portable exoskeleton presented in [33] (Fig. 1), making use of a specific single-phalanx kinematic chain based on a rigid 1 degree of freedom (DOF) mechanism, represents a good trade-off between accuracy and functionality. The high portability of this device demanded for a transmission as compact as possible and the SET positioning (directly on the hand back) required extremely low weight. All these features guarantee the portability of the HES both in rehabilitative and assistive context.

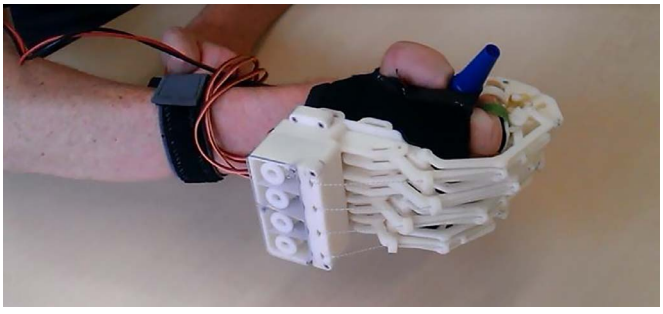

Fig. 1. The first hand exoskeleton prototype, developed by the University of Florence, worn by a patient during the testing phase.

The design of a novel SET has then required the redesign of the whole HES: the ABS-made exoskeleton structure has hence been redesigned for manufacturing in titanium alloy.

In addition, the proposed SET (with its new design method) could be also applied to other mechanisms for different human joints with limited accessibility.

The employment of a SET within the HES leads to important advantages. Indeed, the developed Series Elastic element allows to accurately measure the force exerted on the hand using only angular sensors. Then, an Elastic Transmission implies a compliance, embedded within the system, which softens the device. This is mandatory for a safe exoskeleton, e.g in case of spasms.

Starting from the kineto-static analysis of the finger mechanism, the obtained results have been used to define the quantitative features of the SET. The described in-depth kineto-static analysis has, then, allowed to design the elastic element of the SEA, exploiting innovative topology optimization techniques [34] that were not extensively investigated before in this kind of application.

The experimental validation showed that, thanks to the optimization based design approach, the SET elastic component followed the required features.

The paper is organized as follows. First of all, in Section 2, an overview of the exoskeleton design is reported. The mechanical architecture of the whole system is explained in order to define the application which the SET has been designed to. This particular context has been then taken into consideration throughout the design of the SET. In Section 3, an in-depth analysis of the 1-DOF finger mechanism is presented. The kinematics and the kineto-statics of the mechanism have been studied to define the working conditions for the SET. In particular, the torque required at the actuated joint to achieve the desired movement has been characterized. Section 4 deals with the actuation system. Two strategies exploited to reduce the torque required to actuate the device are reported and explained. In this section, the novel design of the Series Elastic Transmission is illustrated. Finally, in Section 5, the Series Elastic Actuator architecture is given. Focusing on the optimization-based design, a novel elastic element has been characterized and tested.

2. Exoskeleton overview

The HES prototype (shown in Fig. 2a) consists of two main parts: the actuation system and the mechanism of the exoskeleton (Fig. 2b reports an exploded view). As regards the actuation system, two electric servomotors are used to directly actuate joint *A* in both flexion and extension movements. The use of only two motors is justified by the fact that the index is actuated separately with respect to the other three long fingers (middle, ring, little fingers) which are actuated together. This choice allows to greatly improve the portability of the HES without worsening the performance of the device. In fact, while the isolation of the index is strongly important for the precision grip and for the management of the force expressed by the hand, other types of grasp are guaranteed (in terms of functionality) even without a dedicated actuation for each single finger [35,36]. Mechanically, to make possible this solution, the axes of joints *A* of medium, ring and middle fingers are aligned to link them together through a single shaft, with the same actuation system.

The parts of the mechanism are designed, starting from the geometry imposed by the kinetic study, which is reported in Section 3, in order to be built in Ti6Al4V using the Electron Beam Melting (EBM) technology.

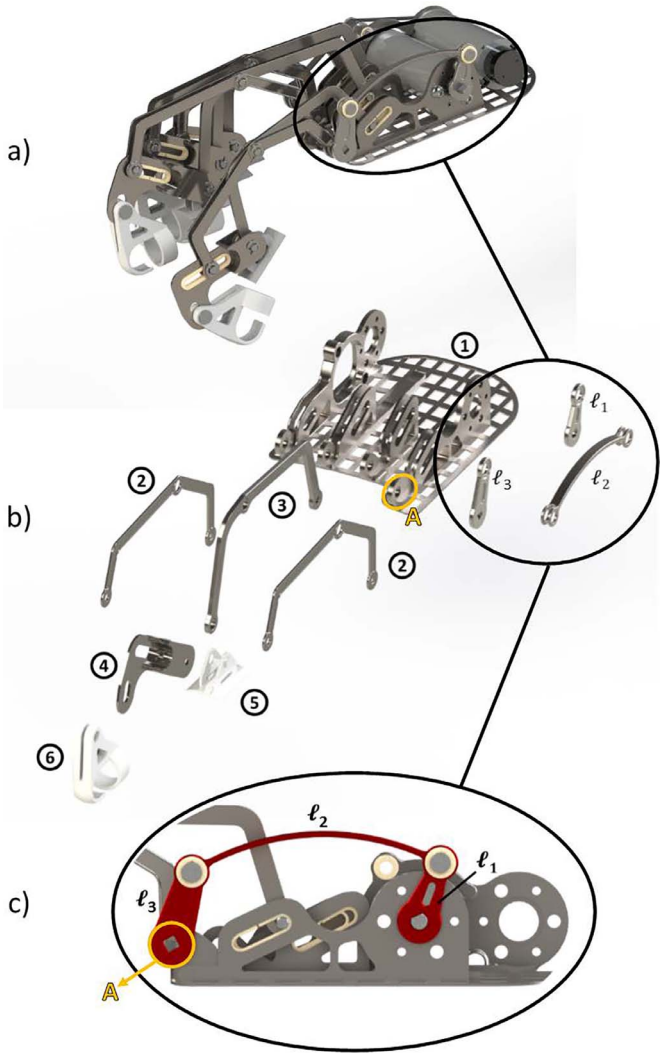

Fig. 2. (a) Designed HES; (b) exploded view drawing; (c) particular: four bar linkage elastic transmission (described in the following).

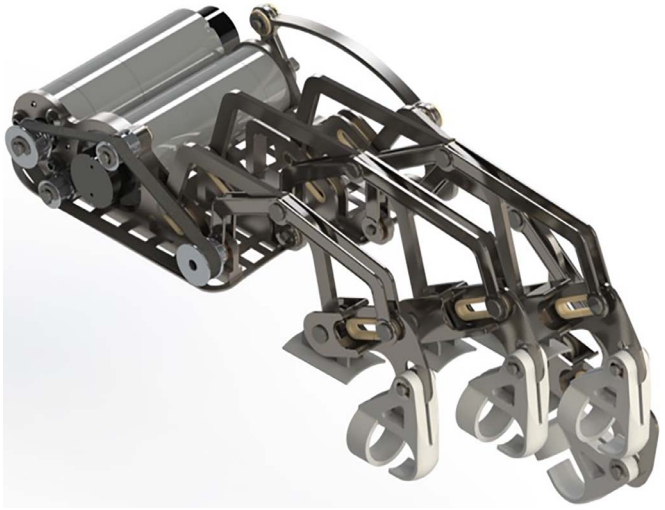

Fig. 3. Realistic render of the HES showing the toothed belt transmission for small, ring and middle fingers actuation.

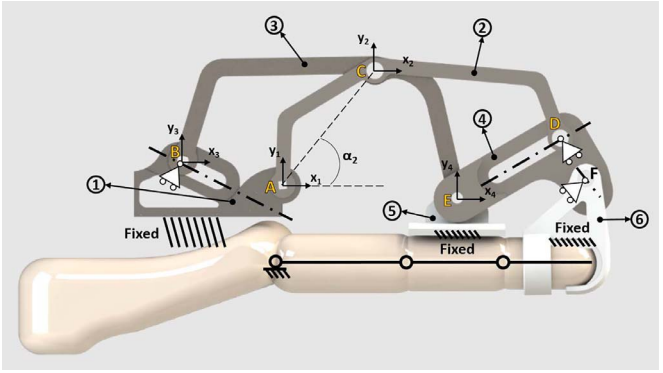

Fig. 4. The 1 DOF mechanism of one finger of the exoskeleton. Black circled numbers indicate the part of the mechanism, yellow capital letters mark each joint. (For interpretation of the references to colour in this figure legend, the reader is referred to the web version of this article.)

Regarding, then, the power transmission from the motors to the joints of the fingers,two different solutions are present. The power transmission on the side of the ring finger uses a toothed belt, as shown in Fig. 3. This choice for small, ring and middle actuation leads to a compact and light transmission. On the other side, the transmission between the finger and the servomotor uses the four bar linkage described in Section 4 (Fig. 7) and shown in Fig. 2c.

In Section 5, the four bar linkage transmission mechanical solution will be explained with particular focus on the Series Elastic component.

3. Mechanism analysis

In this section, the 1 DOF mechanism of the HES (shown in Fig. 4) is outlined. Exploiting the kinematic model of the device, a kineto-static study is reported in order to define the torque required to the actuation system.

As described in details in [33], this specific 1 DOF kinematic chain is able to follow the trajectory of the intermediate phalanx of the hand during both opening and closing gestures. The proposed device (Fig. 2a) can be defined as a rigid single phalanx, single DOF and torque actuated system for the fingers. Each HES feature is defined taking into account the strict requirements of portability and wearability.

The 1 DOF mechanism consist of four main components linked together by means of two 2-DOF joints and three 1-DOF joints.

In order to improve the ergonomics of the exoskeleton, the thimble is added to the mechanism.

When the exoskeleton is worn, body 1 of Figs. 4 and 2 is fixed to the hand back and body 5 is fixed to the intermediate phalanx. The mechanism has 1 active DOF (per finger) to control its kinematics (α_2) when it is placed on the back of the hand. The placement of the actuation system directly on the back of the hand makes possible to activate the mechanism by means of the design of a specific transmission that connects the actuation system and joint A (Fig. 2b and c). This choice improves the portability and the wearability of the device and, in addition, the reliability and the effectiveness of the direct connection between fingers and actuators.

3.1. Kinematics

In order to simplify the analytical description, the focus is on the mechanism of a single finger (in particular the mechanism of the index finger), but the same model and approach can be replicated to study the mechanism of the other long fingers.

The first step of the work is the analysis of the trajectories of the mechanism parts by the use of a kinematic model of the HES. An in-depth analysis of the kinematics of the single-DOF mechanism is detailed in [33]. Nonetheless, the kineto-static analysis, described for the

first time in Section 3.2, required that the kinematic study would have been extended to all joints of the mechanism (in particular, joints F and D which were not included in [33]). A brief overview of the extended kinematics is hence reported hereinafter in order to introduce the kineto-statics.

Referring to Fig. 4, each reference system, characterized in the figure as x_iy_i, will be indicated as $< i >$ in the following, e.g. x_iy_i will be $< 1 >$. Thus, the center of the reference system $< 1 >$ related to body 1 is fixed to the hand (A point). The other reference systems $< 2 >$, $< 3 >$, $< 4 >$ related to bodies 2, 3, 4 are coincident, respectively, with points C, B and E. The kinematic equations describing the mechanism are:

$$\underline{0} = {}^1\underline{C} + R_2^1(\alpha_2)\,{}^2\underline{A} \tag{1}$$

$${}^1\underline{C} = {}^1\underline{B} + R_3^1(\alpha_3)\,{}^3\underline{C} \tag{2}$$

$${}^1\underline{B} + R_3^1(\alpha_3)\,{}^3\underline{E} = {}^1\underline{E} \tag{3}$$

$$a_1\,{}^1B_x + b_1\,{}^1B_y + c_1 = 0 \tag{4}$$

$$a_2\,{}^4D_x + b_2\,{}^4D_y + c_2 = 0 \tag{5}$$

$${}^1\underline{D} = {}^1\underline{C} + R_2^1(\alpha_2)\,{}^2\underline{D} \tag{6}$$

$${}^1\underline{F} = {}^1\underline{E} + R_4^1(\alpha_4)\,{}^4\underline{F}, \tag{7}$$

where referring to Fig. 4, α_i is the rotation of ith frame and e.g. ${}^1\underline{C}$ defines the C point written with respect to the $< 1 >$ reference system.

The unknowns representing the state of the system ${}^1\underline{C}$, ${}^1\underline{B}$, ${}^1\underline{E}$, ${}^1\underline{F}$, ${}^1\underline{D}$, α_2, α_3, α_4 can be calculated as a function of the only one state variable α_2 by solving Eqs. (1)–(7). So, the extended state vector is defined as follows:

$$\underline{q} = [{}^1\underline{B}^T, \alpha_2, {}^1\underline{C}^T, \alpha_3, {}^1\underline{E}^T, \alpha_4, {}^1\underline{F}^T, {}^1\underline{D}^T]^T, \in \mathbb{R}^{13}. \tag{8}$$

All the interesting points of the mechanism (included in the state vector $\underline{q}$) are completely described as functions of the angle α_2 and of the geometrical parameters $\underline{R} \in \mathbb{R}^{16}$:

$$\underline{R} = [{}^2\underline{A}^T, {}^3\underline{C}^T, {}^2\underline{D}^T, {}^3\underline{E}^T, {}^4\underline{F}^T, a_1, b_1, c_1, a_2, b_2, c_2]^T, \tag{9}$$

where e.g. ${}^2\underline{A}$ is the A point written in $< 2 >$ and a_1, b_1, c_1 and a_2, b_2, c_2 are the line equation coefficients (respectively written in the reference frames $< 1 >$ and $< 4 >$) of the mechanism linear constrains. All these parameters are completely known because they represent geometric quantities, depending only on the design of the exoskeleton parts. Consequently, it is possible to solve the extended direct kinematic model $\tilde{\underline{q}} = \underline{f}(\alpha_2, \underline{R}) \in \mathbb{R}^{12}$ (see Eq. (10)) of the mechanism writing a function of α_2 and $\underline{R}$, where $\tilde{\underline{q}}$ is the unknown part of the state vector $\underline{q}$:

$$\tilde{\underline{q}} = \begin{bmatrix} {}^1C_x \\ {}^1C_y \\ {}^1B_x \\ {}^1B_y \\ \alpha_3 \\ {}^1E_x \\ {}^1E_y \\ \alpha_4 \\ {}^1F_x \\ {}^1F_y \\ {}^1D_x \\ {}^1D_y \end{bmatrix} = \underline{f}(\alpha_2, \underline{R}). \tag{10}$$

3.2. Kineto-statics

The first aspect that must be considered in the kineto-static analysis is how much strength is required for the exoskeleton to be exerted.

Determining a suitable output force for the normal manipulation tasks during ADLs is still an important aspect in the hand exoskeletons design. In literature there is a variety of output forces the devices can exert [28,37].

On one side, studies on hand grasping have evaluated that healthy subjects are able to generate a maximum grabbing force up to 300 N (female) and 450 N (male) [37,38]. Such force values result a challenging goal for hand exoskeleton systems, since they demand for a heavy and bulky actuation system, which leads to a non fully portable device. On the other side, when hand impairments occur, these force values decrease and, depending on the severity of the impairment, can be close to zero. With this second aspect in mind, the proposed exoskeleton has not been developed to generate the maximum grip strength of a healthy individual but it has been thought to manipulate object usually handled during the everyday life.

In [39] several objects have been assessed to define benchmarks in grasping and manipulating (e.g. picking up and holding a phone or a mug). Considering a weight target up to 1.5 kg and a coefficient of friction of 0.255 (values determined by Matheus and Dollar [39]), a grabbing force of 14.7 N results suitable in manipulating most of the objects.

Thus, as regards the performance of the HES, each finger mechanism is required to express a 20 N force. This value is identified as a conservative choice and a suitable output for the normal manipulation tasks during ADLs even when only one finger is required in these tasks.

Since the introduction of the thimble produces a second contact point between the hand and the device, in addition to the one on point E, the force of 20 N, required for the output, is split in 2 forces of 10 N each, applied to both contact points, E and F. This assumption guarantees to apply a uniform pressure on the grabbed object. Since the hand exoskeleton studied in this research activity presents only 1 DOF per finger, holding an object becomes mandatory, while controlling and changing the position and orientation of the object could be neglected in this case. Assuming to hold a non-absolutely rigid object, exerting a uniform pressure on it, the object itself initially changes its shape and position with respect to the hand in order to assume a stable pose. Thus, the object results form-closed [40] (i.e. it is impossible to move the object because each point is in contact with the hand) if the stiffness is low and force-closed [40] (i.e. the hand applies forces on the object only through some contact points) if its stiffness is high. However, the aforementioned condition presents the inherent limitation in grabbing very soft objects or objects with an irregular shape. A very soft object could be squeezed too much before reaching the stable position while an objects with an irregular and thin shape might not be grabbed properly. In these cases, the 1-DOF per finger mechanism does not guarantee the required precise grasping procedure.

The kineto-static analysis allows to calculate the torque needed on joint A during the flexion of the HES to express the force of 20 N for each finger. The presented study regards the hand closure, since such movement stresses the most the mechanism. In fact, during the hand extension, the torque required at joint A would take into account only the necessity of lifting the finger.

Hereafter the mathematical procedures for the kineto-static analysis are described.

The direct kinematic model, described in Section 3.1, leads to vector $\underline{\psi}(\underline{q})$ which collects Eqs. (1)–(7), which represent the constrains of the finger mechanism:

$$\underline{\psi} = \begin{bmatrix} {}^1C_x + c\alpha_2{}^2A_x - s\alpha_2{}^2A_y \\ {}^1C_y + c\alpha_2{}^2A_y - s\alpha_2{}^2A_x \\ {}^1B_x + c\alpha_3{}^3C_x - s\alpha_3{}^3C_y - {}^1C_x \\ {}^1B_y + c\alpha_3{}^3C_y + s\alpha_3{}^3C_x - {}^1C_y \\ a_1{}^1B_x + b_1{}^1B_y + c_1 \\ {}^1B_x + c\alpha_3{}^3E_x - s\alpha_3{}^3E_y - {}^1E_x \\ {}^1B_y + c\alpha_3{}^3E_y + s\alpha_3{}^3E_x - {}^1E_y \\ a_2{}^4D_x + b_2{}^4D_y + c_2 \\ {}^1E_x + c\alpha_4{}^4F_x - s\alpha_4{}^4F_y - {}^1F_x \\ {}^1E_y + c\alpha_4{}^4F_y + s\alpha_4{}^4F_x - {}^1F_y \\ {}^1D_x - c\alpha_2{}^2D_x + s\alpha_2{}^2D_y - {}^1C_x \\ {}^1D_y - c\alpha_2{}^2D_y - s\alpha_2{}^2D_x - {}^1C_y \end{bmatrix}. \tag{11}$$

According to Eq. (11), Eqs. (1)–(7) can be written in compact form as

$$\underline{\psi}(\underline{q}, \underline{R}) = \underline{0}. \tag{12}$$

The required torque on joint A is then characterized by the equation:

$$\underline{\gamma}^T \delta \underline{P} = \tau \delta \alpha_2, \tag{13}$$

where $\underline{P}$ is the vector collecting all the application points of the forces applied to the HES and it is defined as follows:

$$\underline{P} = [\underline{P}_A, \underline{P}_B, \underline{P}_C, \underline{P}_D, \underline{P}_E, \underline{P}_F]^T. \tag{14}$$

Vector $\underline{P}$ depends only from α_2 and $\underline{R}$:

$$\underline{P} = \underline{P}(\underline{q}) = \underline{P}(\underline{q}(\alpha_2, \underline{R})) = P(\alpha_2, \underline{R}). \tag{15}$$

Vector $\underline{\gamma}$ collects, in turn, the forces applied to the joints of the mechanism. τ is, finally, the torque required on the joint A.

By means of the kineto-static model of the mechanism, torque τ at joint A is calculated considering, as explained at the beginning of this section, two 10 N forces applied to joints E ($\underline{\gamma}_E$) and F ($\underline{\gamma}_F$).

Considering Eq. (13), τ can be calculated:

$$\tau(\alpha_2, \underline{R}) = \left(\frac{\delta \underline{P}}{\delta \alpha_2}(\alpha_2, \underline{R})\right)^T \underline{\gamma}, \tag{16}$$

where $\left(\frac{\delta \underline{P}}{\delta \alpha_2}(\alpha_2, \underline{R})\right)^T$ is the Jacobian of the mechanism.

Fig. 5 (black line) reports the torque necessary for the flexion of the hand during a complete closure movement. Variable range of

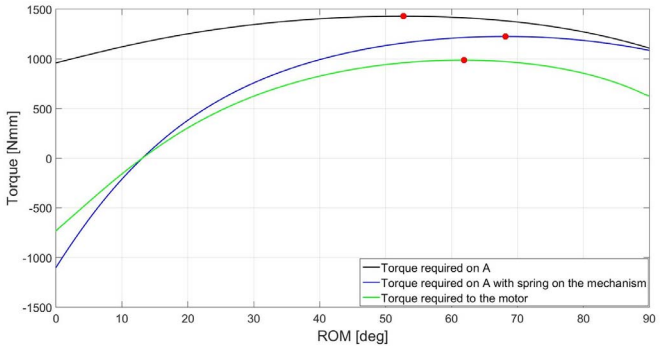

Fig. 5. HES actuation requests: torque on joint A without systems that lower the required actuation in black, torque on joint A when a spring is put between joints D and E in blue, torque required to the motor (with the spring placed on the mechanism) in green. Red dots highlight the maximum value of each requested torque. (For interpretation of the references to colour in this figure legend, the reader is referred to the web version of this article.)

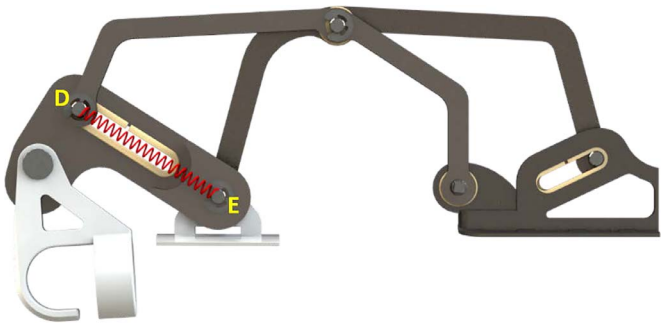

Fig. 6. Lateral view of the 1-DOF mechanism. In red: spring placed between E and D joint for torque reduction. (For interpretation of the references to colour in this figure legend, the reader is referred to the web version of this article.)

movement (ROM) typifies a complete flexion or extension of the finger, whom corresponds 90° of mechanism angle α_2 with. The maximum value, highlighted in red, of the torque is 1430 N mm.

4. Actuation strategy

An electrical servomotor positioned on the back of the hand directly actuates joint A. This choice requires strictly restriction in terms of weight and bulk to get satisfying requirements of portability and wearability. For these reasons, since servomotors as small as possible are mandatory, two systems for reducing the torque at joint *A* were studied and are described in the following.

4.1. Elastic element

The first step is the use of passive elements within the mechanism. In fact, placing an elastic element between joints *D* and *E* of the HES (highlighted in red in Fig. 6) acts a reduction of the torque required in *A*. The behavior of this component is simulated as reported below:

$$\begin{cases} \underline{\gamma}_{Espring} = K(\underline{D} - \underline{E}) \\ \underline{\gamma}_{Dspring} = K(\underline{E} - \underline{D}) \end{cases} \tag{17}$$

where $\underline{\gamma}_{Espring}$ is the force generated by the elastic element on joint *E*, $\underline{\gamma}_{Dspring}$ is the force of the elastic element on joint *D* and *K* is the stiffness of the spring.

So, vector $\underline{\gamma}$ can be written as:

$$\underline{\gamma} = \left[\underline{0}, \underline{0}, \underline{0}, \underline{\gamma}_{Dspring}, \underline{\gamma}_E + \underline{\gamma}_{Espring}, \underline{\gamma}_F\right]^T, \in \mathbb{R}^{12} \tag{18}$$

where the first three vector elements are equal to zero because they represent external forces applied to *A, B* and *C* joints, which are not loaded. While $\underline{\gamma}_E$ and $\underline{\gamma}_F$ are two vectors representing the external grasping forces (10 N each) applied to *E* and *F* joints, respectively. The maximum reduction of the highest value of the torque is yielded by the optimum value of K, which is indicated as K_{opt} in the following. The optimization procedure of Eq. (16) with respect to the parameter *K* is

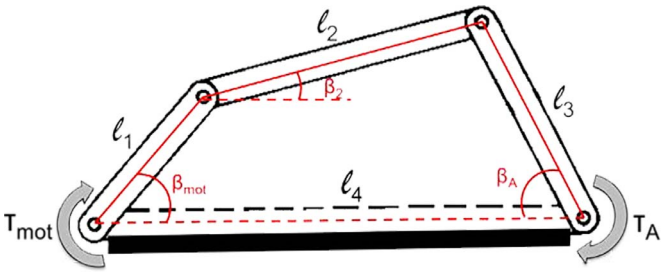

Fig. 7. Geometrical scheme of the four bar linkage.

described below.

Once the elastic element has been added (Eq. (18)), Eq. (16) can be written as:

$$\tau(\alpha_2, \underline{R}, K) = \left(\frac{\delta \underline{P}}{\delta \alpha_2}(\alpha_2, \underline{R})\right)^T \underline{\gamma}(\alpha_2, \underline{R}, K), \tag{19}$$

where the dependence of τ by K is clear.

The element optimum stiffness is, then, given by:

$$K_{opt} = \arg\min_{K}\left(\max_{\alpha_2} |\tau(\alpha_2, \underline{R}, K)|\right), \tag{20}$$

where $\max_{\alpha_2} |\tau(\alpha_2, \underline{R}, K)|$ is the objective function to be minimized and K_{opt} is calculated as that stiffness which minimizes the maximum value of the torque reached in the whole ROM (represented by α_2).

The optimization problem has been solved exploiting the MATLAB® Optimization Toolbox, in particular the Levenberg–Marquardt algorithm [41] and leads to a value of the elastic element stiffness of 1.7 N/mm.

Fig. 5 (blue line) reports the torque necessary for the flexion of the hand with the interposition of the elastic element between joints *D* and *E*. The addition of the spring causes a lowering of the maximum value of the torque required at the joint *A* from 1430 N mm to 1220 N mm.

4.2. Four bar linkage

A further reduction of the required torque is reached thanks to the design of a four bar linkage between the output shaft of the servomotor and joint *A*. Considering the geometrical scheme reported in Fig. 7, and if the frictional forces at the joints are negligible, it is possible to write:

$$\tau_{mot}\delta\beta_{mot}(\underline{\ell}) + \tau(\alpha_2)\delta\beta_A(\underline{\ell}) = 0, \tag{21}$$

where $\underline{\ell}$ is the vector collecting the axial lengths of the four bar linkage components.

Since

$$\beta_A = \alpha_2 + c,$$

where c is a constant defined by the geometry of the transmission,

$$\delta\beta_A = \delta\alpha_2. \tag{22}$$

So, the output torque from the servomotor is

$$\tau_{mot} = -\tau(\alpha_2, \underline{R})\frac{d\beta_A(\underline{\ell})}{d\beta_{mot}(\underline{\ell})}, \tag{23}$$

where $i = \frac{d\beta_A}{d\beta_{mot}}$ is the transmission ratio of the mechanism.

Since i changes depending on the pose of the HES, which depends on the parameter α_2 (DOF of the mechanism) as reported in Eq. (22), then, i itself is a function of α_2 and its value changes during the opening and closure movements of the device. Therefore, the transmission is analysed during the whole ROM of the HES in order to obtain the trend of τ_{mot} depending on the trend of τ_A, which is a function of the only state variable α_2. Refer to Eq. (23) and, in particular, to $\underline{\ell}$. Since ℓ_4 length is constrained by design features (distance between servomotor shaft and A joint is set), the only state variable which properly describes the linkage behavior is $\frac{\ell_3}{\ell_1}$ ratio. Components size reported in Table 1 leads to a reduction of 30.8% of the required torque, with a maximum value of the torque equal to 990 N mm (Fig. 5). This analysis considers also the use of the spring described before.

Table 1
Four bar linkage characteristics (mm).

Component	Size
ℓ_1	15
ℓ_2	60
ℓ_3	18
ℓ_4	59.9

5. Series Elastic Actuator design

In this specific application, the relevance of SEA strategy is considerably important due to the compliance of the transmission, which introduces safety and comfort in wearing the exoskeleton, reduces the possibility of causing pain when potential spasms occur and, last but not least, produces an exact measurement of the applied force without having standard force sensors.

The choice of a suitable value for the stiffness of the transmission will be defined through the setting of upper and lower limits. Such stiffness, included in a specific range, guarantees a suitable torque control characterized by the resolution of the encoder for the upper limit, and by a limited strain of the elastic component during the use of the device. This will be explained in details in the following.

This Section is divided into three parts. In the first part, a kinetostatic analysis of the four bar linkage is given. This analysis allows for the determination of the design specifications, which are exploited in the second part to design an elastic component of the SET with predefined features. In the last part, the experimental procedure to characterize the component and the related results are reported.

5.1. SEA: design specifications

The index, because of its proximity to the thumb, is the most relevant and dexterous among the hand long fingers [42] and it is the finger required to manipulate objects dexterously. Several studies have noted its importance in precision pinch and directional grip [43,44]. For all these reasons, the integration of a SEA within the exoskeleton has been limited to its mechanism.

The element ℓ_2 of the four bar linkage (Fig. 7) serves as elastic element of the Series Elastic Actuator for the closed-loop control (Fig. 8).

In order to reduce as much as possible the overall dimensions of the mechanism with the suitable torque reduction factor already identified in Section 4, the dimensions of the element ℓ_2 are those ones reported in Table 1.

In the well-known SEA control architecture [23], a controller, exploiting the measured deformation of the elastic component, is in charge of managing the actuator to track the set torque value to the moving linkage of the exoskeleton. In the position controller, the

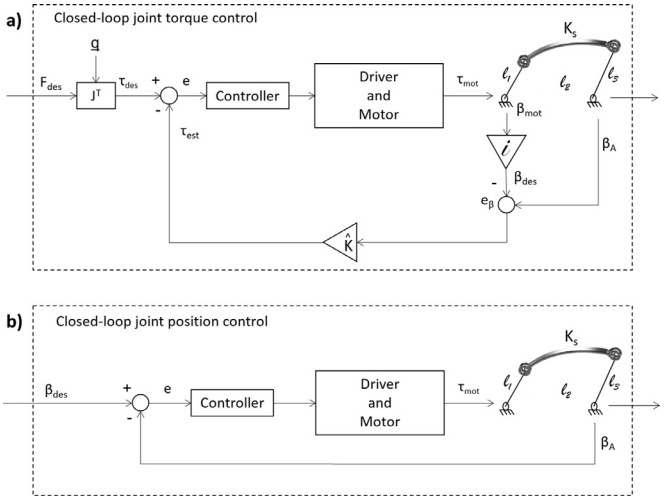

Fig. 8. Scheme of the SEA torque (a) and joint position (b) closed-loop control. i and $\widehat{K}$ are the gear ratio and the torsional stiffness of the transmission, respectively, J is the Jacobian matrix of the mechanism, K_s is the stiffness of the element ell_2 and $\underline{q}$ is the state vector of the extended kinematics of the mechanism.

control loop is closed on the angular encoder placed in the four-bar linkage mechanism (Fig. 8). The torque control requires that the mechanical features of the elastic element must be as close as possible to the designed ones. To obtain what is mentioned above, the SEA in-series elasticity was realized by a custom elastic element, which achieves a suitable stiffness and bears the stress up to the design value without neither yielding, nor presenting hysteretic or non-linear behavior.

Regarding the definition of the optimum value of the spring stiffness, the upper and lower limits of that value were studied to allow the spring to perform a suitable torque control. In particular, the upper limit (maximum stiffness) takes into account the resolution of the encoder for the angular measurement. Torque control is performed by the measurement of the angle value

$$e_\beta = \beta_A - \beta_{des}. \tag{24}$$

This measurement exploits two encoders: one positioned on the motor for β_{mot} (and therefore traceable to β_{des}), the other on joint A for β_A. The higher is the spring stiffness, the higher must be the encoder resolution to measure very small angular variations.

As regards the stiffness lower limit, this is given by the geometry of the mechanism. In fact, a too low value of stiffness would lead to a strongly irregular behavior of the transmission structure which would be impossible to manage with the feedback control.

To define the upper and lower limits, the power transmission kineto-static model has been implemented in MATLAB®environment. In particular, the elastic element ℓ_2 has been modeled as follows:

$$\ell_2^{eff} = \ell_2^{start} + \frac{T}{K_s} \tag{25}$$

where ℓ_2^{eff} is the length of the element ℓ_2 taking into consideration its strain. That depends on the force T which acts on its axis during the actuation, ℓ_2^{start} is the length of the element ℓ_2 when there is no strain and K_s is the stiffness of the component.

Therefore, referring to Fig. 7, the following equations represent the kineto-static model of the system:

$$\begin{cases} \ell_1 c\beta_{mot} + \left(\ell_2^{start} + \dfrac{T}{K_s}\right) c\beta_2 + \ell_3 c\beta_A = \ell_4 \\ \ell_1 s\beta_{mot} + \left(\ell_2^{start} + \dfrac{T}{K_s}\right) s\beta_2 + \ell_3 s\beta_A = 0 \\ T = \dfrac{\tau_{mot}}{\ell_1 s(\beta_{mot} - \beta_2)} \\ T = \dfrac{\tau_A}{\ell_3 s(\beta_2 + \beta_A)} \end{cases} \tag{26}$$

where c and s are, respectively, *cos* and *sin* of the angle on their right.

To define the lower limit for the value of ℓ_2 stiffness, the system of Eq. (26) has been implemented. The model receives as input vector $\underline{\tilde{q}}$ from the direct kinematic model, the torque τ_a from the kineto-static model and a set value K_s of ℓ_2 stiffness and it returns in output the value of τ_{mot}, T and the angles β_{mot} and β_2.

This analysis allowed to identify the lower limit of the value of K_s equal to 60 N/mm. For lower values, there are deformations of the element ℓ_2 such as to cause an undesired trend of the output torque of the servomotor. In these cases, much energy gets stored by the spring and causes a noteworthy deformation on the elastic element. This yields, in the latest phase of the closing gesture, a high variation of the angle β_A with respect to a low variation of the ROM. The higher is the degree of change of β_A angle, the higher is the one of the required torque τ_{mot} (see Eq. (23)). This would require very high performance by the controller and, consequently, by the motor as well.

Fig. 9 graphically explains the aforementioned behavior. Considering a K_s stiffness of 58 N/mm (black dotted trend), which is just below the identified lower limit, when the hand is almost closed, around 90° of ROM, a small closure corresponds to a very high degree of change of β_A angle. The motor, in turn, should track a far reference in torque in a limited time. Considering, instead, a more rigid component (e.g. with a stiffness of 100 N/mm), both degrees of change, one of β_A and the other of motor torque, are lower. This demands for a smother behavior of the controller.

As regards the definition of K_s upper limit, the same function receives as input vector $\underline{\tilde{q}}$ from the direct kinematic model, a trend of the torque τ_A varying linearly between 0.5 N m and −0.5 N m and the set value K_s of ℓ_2 stiffness. Such linear trend of the torque has been applied to joint A to find out a maximum value of K_s that allows the evaluation of an angular value on that joint itself.

The results are reported in Fig. 10. The torque applied to joint A depends on the angle β_A. So, this torque depends also on the system parameter of the mechanism (angle α_2), which defines the pose of the HES.

Focusing on the X–Z plane (Fig. 11), it is possible to identify the straight line with the maximal slope (highlighted in red). This line represents the pose of the HES during which the minimal angular variation causes the maximum precision in evaluating of the torque on joint A.

The set torque applied to joint A is in relation to β_A as reported below:

$$\tau_A = \widehat{K}\beta_A \Rightarrow \Delta\tau_A = \widehat{K}\Delta\beta_A, \tag{27}$$

where $\widehat{K}$ is the torsional stiffness of the transmission which is a function only of the element ℓ_2 stiffness (K_s) if the elements ℓ_1 and ℓ_3 do not warp.

The angular resolution of the encoder ($\Delta\beta_A$) is associated to the resolution in terms of the SEA torque; that depends on the value of K_s. With a spring having a stiffness K_s = 100 N/mm it is possible to evaluate, using an encoder with 4096 steps per revolution, an angular variation of 0.088° and therefore it is possible to measure a torque up to 0.049 N mm. Higher values of stiffness involve, at the same angular resolution, a higher value of torque variation which, as explained in the following, has not been considered by the authors as suitable to be managed in the closed-loop torque control. Referring to Eq. (27), with a set resolution of the encoder ($\Delta\beta_A$), the higher the stiffness of the transmission is (considering a linear-elastic behavior of the component), the higher the minimum measurable variation in the torque is (τ_A). Thus, if the in-series elastic element were totally rigid, no torque variation would be appreciated and the force controller would not be implementable. With this in mind, the upper limit value of 100 N/mm has been chosen in order to keep the resolution of the torque controller under 0.05 N mm. An additional increase of the stiffness of the elastic element would have further lowered the performances of the controller.

Fig. 9 reports the output torque of the motor (red dotted line), necessary to express a force of 20 N on the index, in case of a stiffness of the elastic element of 100 N/mm.

5.2. SEA: topology optimization

The design of a mechanical component with defined specifications, in terms of size (60 mm axial) and stiffness (within a range from 60 to 100 N/mm), is achieved by means of a topology optimization method [34,45].

In this case, for the topology optimization technique, whose scheme is reported in Fig. 12, software *Altair Hyperworks* has been used.

The most important steps followed during the optimization analysis are written hereinafter.

5.2.1. Test case definition

Starting from the geometric features of the component, a static analysis is applied on a non-optimized version of the component ℓ_2 (baseline model in Fig. 12) in order to get a benchmark useful for the optimization.

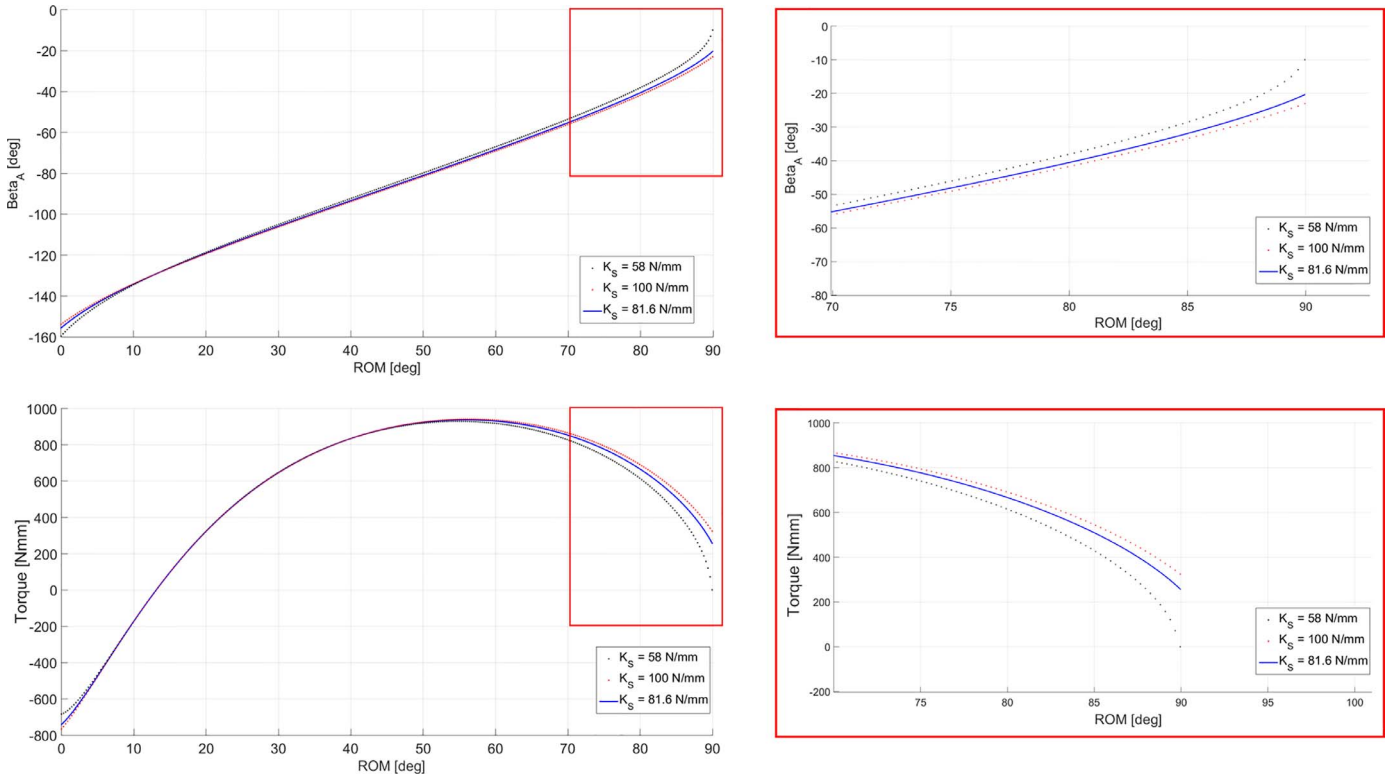

Fig. 9. Trend of β_A angle (on top) and torque required to the motor (on bottom) with respect to the ROM. Red, blue and black lines report the behavior of the system when the stiffness of the elastic element is 60 (lower limit), 81.6 (optimum value) and 100 (upper limit) N/mm respectively. On the right, the effect of the stiffness parameter K_s on the trends of β_A and of the torque required to the motor is highlighted. (For interpretation of the references to colour in this figure legend, the reader is referred to the web version of this article.)

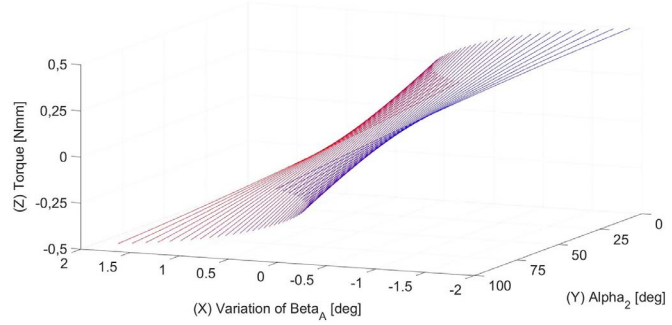

Fig. 10. Angular variation on the joint A depending on the set torque and on the pose of the HES.

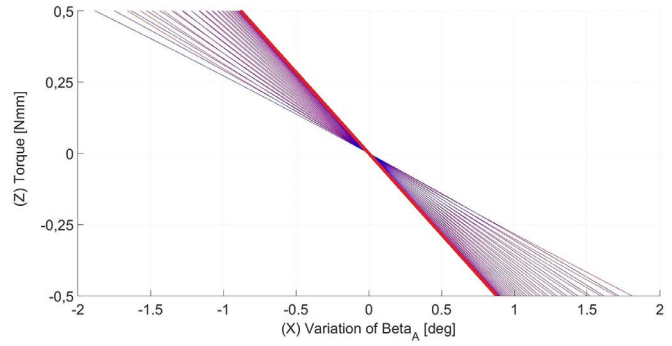

Fig. 11. Torque on joint A depending on the angular variation of the same joint. (For interpretation of the references to colour in the text, the reader is referred to the web version of this article.)

The static analysis has been set by imposing an axial load of 90 N. Such a value is the load that the component bears during the use of the device and has been calculated using Eq. (26), varying the stiffness of the in-series elastic component within the range between 60 and 100 N/mm—range bounded by the minimum and maximum values for the stiffness. In addition, the component has been constrained such as to replicate its real configuration on the four bar linkage.

The value of ℓ_2 stiffness is obtained from the finite element analysis through the axial displacement measurement caused by the load:

$$K_s = \frac{T}{u_a} \tag{28}$$

where, again, K_s is ℓ_2 stiffness, T is the load applied to element ℓ_2 and u_a is the axial displacement of element ℓ_2.

For the static analysis the material model has linear elastic isotropic properties. The material properties are indicated in Table 2.

5.2.2. Design space definition

In the topology optimization, the design area denotes the set of elements that may be removed during the optimization, in contrast to the non-design space that remains unchanged.

The region around the holes must be kept as it is, so belonging to the non-design space and it does not change after the topology optimization.

5.2.3. Objective function definition

In the formulation of optimization problems, some quantities can be used as objective function to be minimized (usually global quantities) and some others as constraints (usually local quantities): volume (or volume fraction), mass (or mass fraction), displacements, stresses and strains. The minimization of the objective functions is imposed to have a new optimized geometry and the minimization of the volume has been tested in this work:

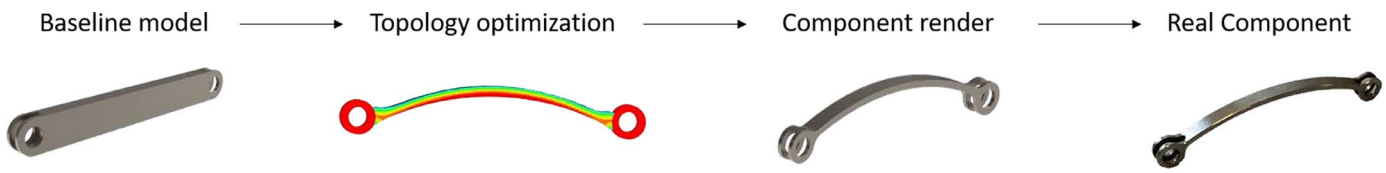

Fig. 12. Topology optimization procedure.

Table 2
Material properties.

Young's modulus (E)	$120*10^3$ MPa
Poisson's ratio (ν)	0.342
Density (ρ)	4.43 g/cm^3

Table 3
Finite element analysis results.

σ_{max}	423.9 MPa
Mass	2.4 g
u_a	1.1 mm

$$V(\rho_f) = \int_\Omega \rho_f d\Omega \tag{29}$$

where ρ_f is the material density and Ω is the domain. The optimization constraints used in this work are on the displacements and on the maximum value of the stress. The various constraints could be defined as follows:

$$\begin{cases} \sigma_{max} \leq \sigma_y \\ u_{max} \geq u_a \geq u_{min} \end{cases} \tag{30}$$

where:

- σ_{max} is the maximum allowable value of stress in the optimized model;
- σ_y is the maximum acceptable value of stress to be set in the optimization test and it is equal to the yield strength of Ti6Al4V (930 MPa);
- u_{max} is the maximum axial displacement to be set during the optimization test, this value is set equal to 2.2 mm to reach a stiffness of 60 N/mm;
- u_{min} is the minimum axial displacement to be set during the optimization test, this value is set equal to 1.3 mm to reach a stiffness of 100 N/mm;
- u_a is the maximum axial displacements allowable in the optimized model (this is the control parameter used to define the axial stiffness of the elastic element, as explained through Eq. (28)).

5.2.4. Topology optimization

Hereinafter, the results concerning the topology optimization with the best performance are reported.

The stiffness of the obtained Finite Element model results 78.8 N/mm. The carried out analysis allowed to design the component ℓ_2 as shown in Fig. 12.

Then, a finite element model of the optimized component was studied using the software *Altair HyperWorks*. A load of 90 N in compression and traction was applied to the model in the axial direction. The constraints are the same of the previous models. The finite element analysis (FEA) results are shown in Table 3.

The FEA shows the correspondence of the model characteristics to the design specifications. In particular, it presents a value of axial stiffness (it is equal during the compression and the traction) of 80.6 N/mm.

The maximum stress makes safe the structure both for static and fatigue analysis.

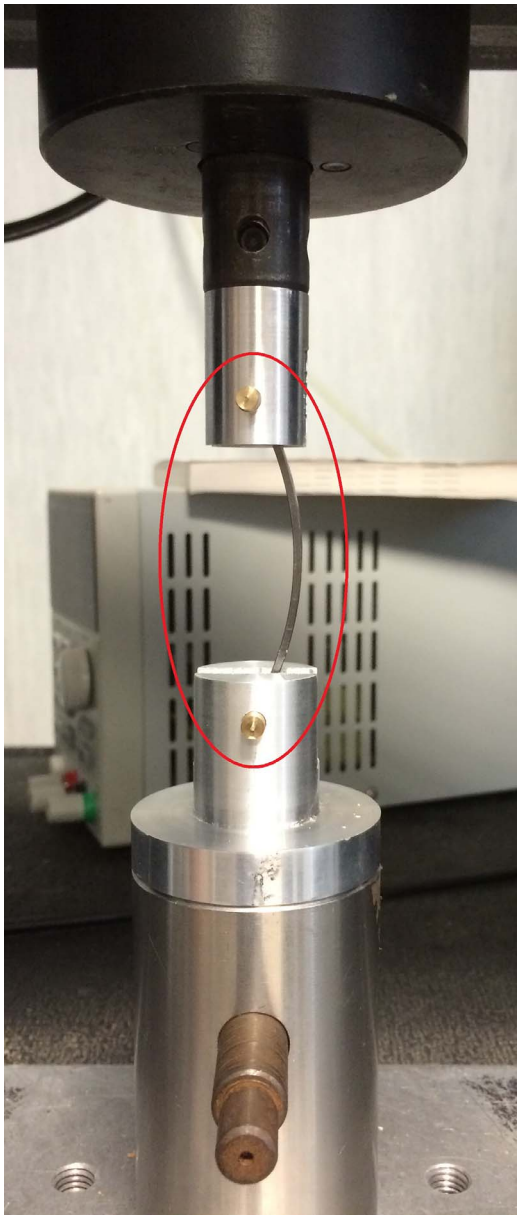

Fig. 13. Test setup.

5.2.5. Finite element analysis of the transmission

Since the control architecture of the SEA considers the angular variation between the angles β_{des} and β_A due to the stiffness of the entire transmission system, a finite element model of the entire four bar linkage was developed.

The model was tested with the calculated torque τ_A (blue trend in Fig. 5) applied to element A.

Each component was linked to each other such as to replicate the real configuration of the four bar linkage.

The results of FEA shows that the transmission system, under the set load program and constraints, presents an axial stiffness K_s = 77.3N/

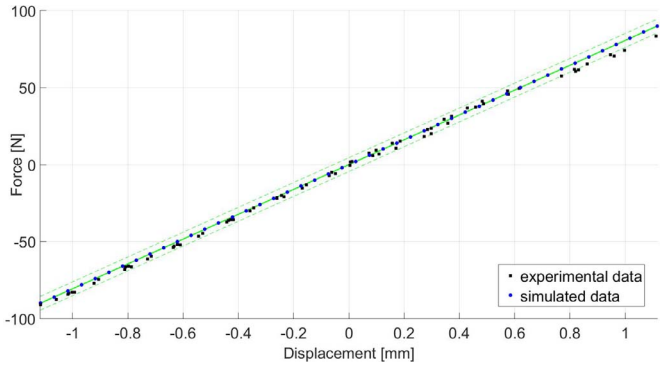

Fig. 14. Simulated data are represented with blue circle dots, while experimental data are represented with black square dots (resampled at 0.55% to make them visible). The stiffness (calculated as the inverse of the slope of the linear regression curve) is equal to 80.6 N/mm for the simulated elastic module and 81.8 N/mm for the real component. (For interpretation of the references to colour in this figure legend, the reader is referred to the web version of this article.)

mm. This is due to the small strain of the components ℓ_1 and ℓ_3. However, the angular variation, caused by the deformation of the components ℓ_1 and ℓ_3 is smaller than the minimum value that the encoders are able to read, so, their deformations do not affect the measurement.

Referring to the new value of stiffness of element ℓ_2, the output torque of the motor, necessary to express a force of 20 N on the index, is shown in Fig. 9 (blue trend).

5.3. SEA: experimental results

The experimental characterization of the designed elastic component has been conducted using a custom-made connection to the Instron testing machine (Instron 3365, INSTRON Inc., Norwood, MA, US load cell, Full Scale: 500 N, accuracy in force regulation of 0.5%). Fig. 13 reports the test bed setup. The elastic element has been characterized by applying 10 cycles of increasing value of force from − 90 N (compression of the component) to 90 N (traction of the component), with increments of 0.5 mm/min in both the directions. Ten tests have been performed for each 10 cycles of applied load, allowing the element to recover the unperturbed position after each trial.

In Fig. 14, the load versus displacement of the experimental and simulated data are plotted. In addition, on the same plot, data from FEM simulations are interpolated with a linear regression represented with a solid line ($R^2 = 1$); its 95% confidence interval is reported in the same figure. FEM simulations data would predict a stiffness $K_{sim} = 80.6$ N/mm, while the measurements indicated a stiffness $K_{real} = 81.8$ N/mm, corresponding to an error between simulated data and measured data, calculated as $(k_{real} - k_{sim})/k_{sim}100$, equal to 1.5%.

Since the experimental data result quite scattered around the linear regression curve of simulated data, the evaluation of the actual stiffness deserves further experimental investigation, as discussed in Section 6.

6. Conclusion and further developments

The proposed research work aims at developing a novel Hand Exoskeleton System for hand disabilities. In this paper, particularly, the modeling, design and testing phase of the Series Elastic Transmission, put within the device mechanical structure, were presented.

Starting from the 1-DOF finger mechanism developed by the University of Florence, a new robotic device has been designed. This exoskeleton, thought to be manufactured in a suitable Titanium alloy (Ti6Al4V) by means the Electron Beam Melting (EBM) technology, exploits a novel power transmission, never used before in this field, based on Series Elastic Actuator to actuate and control the index finger mechanism. The particular optimized four bar linkage structure leads to an important reduction in terms of required torque from the actuation system.

The kineto-static model of a specific transmission component has been studied and its shape has been optimized, using topology optimization techniques, to precisely obtained the set stiffness value, which allows the SEA to work properly.

The transmission addressed innovative features related to its particular work conditions. In fact, thanks to the topology optimization process, its mechanical characteristics have been “tailored” to the real use of the component. These characteristics satisfy important design requirements for an assistive device:comfortable human-robot physical interface capable to transmit the assistive torque; safe and effective actuation and control systems.

An experimental characterization has been performed to validate the finite element analysis and to assess the effectiveness of the elastic component. This phase highlights that the elastic component is able to withstand the operating conditions (the maximum load applied was 90 N), with a constant stiffness of 81.8 N/mm, in agreement with FEAs performed, which predicted a stiffness value of 80.6 N/mm. However, when the component was stressed over 60 N, the experimental data have highlighted a behavior that is not extremely close to the FEAs results. For this reason, as regards future work, further investigation is scheduled. In particular, experimental tests on the whole transmission system will be scheduled. Finally, the realization of the entire HES will allow to test the Series Elastic Transmission in more complicated working conditions replicating real scenarios.

References

[1] Benjamin EJ, et al. Heart disease and stroke statistics—2017 update: a report from the american heart association. Circulation 2017;135(10):e1–459.
[2] Parkinson’s Disease Foundation. Statistics for Parkinson’s Disease. 2017. http://www.pdf.org.
[3] Arthritis Foundation. Arthritis facts. 2017. http://www.arthritis.org.
[4] Pons J. Rehabilitation exoskeletal robotics. The promise of an emerging field. IEEE Eng Med Biol Mag 2010;29(3):57–63.
[5] Nakayama H, Jørgensen H, Raaschou H, Olsen T. Recovery of upper extremity function in stroke patients: the Copenhagen stroke study. Arch Phys Med Rehabil 1994;75(4):394–8.
[6] Kwakkel G, Kollen B, van der Grond J, Prevo A. Probability of regaining dexterity in the flaccid upper limb: impact of severity of paresis and time since onset in acute stroke. http://stroke.ahajournals.org/content/34/9/2181.
[7] Alami R, Albu-Schaeffer A, Bicchi A, Bischoff R, Chatila R, De Luca A, et al. Safe and dependable physical human-robot interaction in anthropic domains: state of the art and challenges. Proceedings of the IEEE/RSJ international conference on intelligent robots and systems (IROS), Beijing, China. 2006. p. 1–16.
[8] Pervez A, Ryu J. Safe physical human robot interaction-past, present and future. J Mech Sci Technol 2008;22(3):469–83.
[9] Vallery H, Veneman J, van Asseldonk J, Ekkelenkamp R, Buss M, van Der Kooij H. Compliant actuation of rehabilitation robots. IEEE Rob Autom Mag 2008;15(3):60–9.
[10] De Santis A, Siciliano B, De Luca A, Bicchi A. An atlas of physical human–robot interaction. Mech Mach Theory 2008;43(3):253–70.
[11] Zhao H, Jalving J, Huang R, Knepper R, Ruina A, Shepherd R. A helping hand: soft orthosis with integrated optical strain sensors and EMG control. IEEE Rob Autom Mag 2016;23(3):55–64. http://dx.doi.org/10.1109/MRA.2016.2582216.
[12] Yap H, Lim J, Goh J, Yeow C. Design of a soft robotic glove for hand rehabilitation of stroke patients with clenched fist deformity using inflatable plastic actuators. J Med Devices 2016;10(4). http://dx.doi.org/10.1115/1.4033035.
[13] Kim B, In H, Lee D, Cho K. Development and assessment of a hand assist device: gripit. J Neuroeng Rehabil 2017;14(1):15. http://dx.doi.org/10.1186/s12984-017-0223-4.
[14] In H, Byunghyun Kang B, Sin M, Cho K. Exo-Glove: a wearable robot for the hand with a soft tendon routing system. IEEE Rob Autom Mag 2015;22(1):97–105. http://dx.doi.org/10.1109/MRA.2014.2362863.
[15] Xiloyannis M, Cappello L, Binh KD, Antuvan CW, Masia L. Preliminary design and control of a soft exosuit for assisting elbow movements and hand grasping in activities of daily living. J Rehabil Assistive Technol Eng 2017. http://dx.doi.org/10.1177/2055668316680315.
[16] Jamwal P, Xie S, Hussain S, Parsons J. An adaptive wearable parallel robot for the treatment of ankle injuries. IEEE/ASME Trans Mechatron 2014;19(1):64–75.
[17] Albu-Schaffer A, Ott C, Hirzinge G. A unified passivity-based control framework for position, torque and impedance control of flexible joint robots. Int J Rob Res 2007;26(1):23–9.
[18] Cianchetti M, Ranzani T, Gerboni G, De Falco I, Laschi C, Menciassi A. STIFF-FLOP surgical manipulator: mechanical design and experimental characterization of the single module. Proceedings of the IEEE/RSJ international conference on intelligent

robots and systems (IROS), Tokyo, Japan. 2013. p. 3576–81.
[19] Hadi A, Alipour K, Kazeminasab S, Amerinatanzi A, Elahinia M. Design and prototyping of a wearable assistive tool for hand rehabilitation using shape memory alloys. ASME 2016 conference on smart materials, adaptive structures and intelligent systems, Vermont, USA. 2016.
[20] Kim S, Kim J, Ryu J. Adaptive energy-bounding approach for robustly stable interaction control of impedance-controlled industrial robot with uncertain environments. IEEE/ASME Trans Mechatron 2014;19(4):1195–205.
[21] Ham R, Sugar T, Vanderborght B, Hollander K, Lefebe D. Compliant actuator designs. IEEE Rob Autom Mag 2009;16(3):81–94.
[22] Chiri A, Giovacchini F, Vitiello N, Cattin E, Roccella S, Vecchi F, et al. HANDEXOS: towards an exoskeleton device for the rehabilitation of the hand. IEEE/RSJ international conference on intelligent robots and systems (IROS), St. Louis, MO, USA. 2009. p. 1106–11.
[23] Pratt G, Williamso M. Series elastic actuators. Proceedings of the IEEE/RSJ international conference on intelligent robots and systems (IROS), Edmonton, Canada. 2005. p. 399–406.
[24] Cempini M, Giovacchini F, Vitiello N, Cortese M, MoisÃÍ M, Posteraro F, et al. NEUROExos: a powered elbow orthosis for post-stroke early neurorehabilitation. Proceedings of the IEEE EMBS international conference (EMBC), Osaka, Japan. 2010. p. 342–5.
[25] Giovacchini F, Vannetti F, Fantozzi M, Cempini M, Cortese M, Parri A, et al. A lightweight active orthosis for hip movement assistance. Rob Auton Syst 2015;73:123–34.
[26] Sergi F, Accoto D, Carpino G, Tagliamonte N, Guglielmelli E. Design and characterization of a compact rotary Series Elastic Actuator for knee assistance during overground walking. Proceedings of the IEEE EAS and EMBS international conference on biomedical robotics and biomechatronics (BioRob), Rome, Italy. 2012. p. 1931–6.
[27] Jo I, Bae J. Design and control of a wearable hand exoskeleton with force-controllable and compact actuator modules. IEEE international conference on robotics and automation (ICRA), Seattle, Washington, USA. 2015. p. 5596–601.
[28] Heo P, Gu G, Lee S-J, Rhee K, J. K. Current hand exoskeleton technologies for rehabilitation and assistive engineering. Int J Precis Eng Manuf 2012;13(5):807–24.
[29] Jones C, Wang F, Morrison R, Sarkar N, Kamper D. Design and development of the cable actuated finger exoskeleton for hand rehabilitation following stroke. IEEE/ASME Trans Mechatron 2014;19(1):131–40.
[30] Cempini M, Cortese M, Vitiello N. A powered finger-thumb wearable hand exoskeleton with self-aligning joint axes. IEEE/ASME Trans Mechatron 2015;20(2):705–16.
[31] Borboni A, Mor M, Faglia R. Gloreha-hand robotic rehabilitation: design, mechanical model, and experiments. J Dyn Syst Measure Control 2016;138(11). http://dx.doi.org/10.1115/1.4033831.
[32] Ma Z, Ben-Tzvi P. RML Glove-An exoskeleton glove mechanism with haptics feedback. IEEE/ASME Trans Mechatron 2015;20(2):641–52.
[33] Conti R, Meli E, Ridolfi A. A novel kinematic architecture for portable hand exoskeletons. Mechatronics 2016;35:192–207.
[34] Bendsoe MP, Sigmund O. Topology optimization: theory, methods and applications. Berlin, Germany: Springer-Verlag; 2003.
[35] Iberall T. Grasp planning from human prehension. Proceedings of the 10th international joint conference on artificial intelligence (IJCAI), Milan, Italy. vol. 2. 1987. p. 1153–6.
[36] Feix T, Romero J, Schmiedmayer H, Dollar A, Kragic D. The GRASP taxonomy of human grasp types. IEEE Trans Hum Mach Syst 2016;46(1):66–77. http://dx.doi.org/10.1109/THMS.2015.2470657.
[37] Dovat L, Lambercy O, Gassert R, Maeder T, Milner T, Leong T, et al. Handcare: a cable-actuated rehabilitation system to train hand function after stroke. IEEE Trans Neural Syst Rehabil Eng 2008;16(6):582–91. http://dx.doi.org/10.1109/TNSRE.2008.2010347.
[38] Mathiowetz V, Kashman N, Volland G, Weber K, Dowe M, Rogers S. Handcare: a cable-actuated rehabilitation system to train hand function after stroke. IEEE Trans Neural Syst Rehabil Eng 1985;66(2):69–74.
[39] Matheus K, Dollar A. Benchmarking grasping and manipulation: properties of the objects of daily living. IEEE/RSJ international conference on intelligent robots and systems (IROS), Taipei, Taiwan. 2010. p. 5020–7.
[40] Prattichizzo D, Trinkle JC. Grasping. Handbook of robotics. New York: Springer; 2016. p. 955–88.
[41] Moré JJ. The Levenberg-Marquardt algorithm: implementation and theory. Berlin, Heidelberg: Springer; 1978. p. 105–16. http://dx.doi.org/10.1007/BFb0067700. ISBN 978-3-540-35972-2
[42] Duncan SF, Saracevic CE, Kakinoki R. Biomechanics of the hand. Hand Clin 2013;29(4):483–92.
[43] Tubiana R, Thomine J, Mackin E. Movements of the hand and wrist. Examination of the hand and wrist. 1996. p. 40–125.
[44] Duparc J, Alnot J-Y, May P. Single digit amputations. Mutilating injuries of the hand. 1979. p. 37–44.
[45] Wang M, Wang X, Guo D. A level set method for structural topology optimization. Comput Methods Appl Mech Eng 2003;192:227–46. http://dx.doi.org/10.1016/S0045-7825(02)00559-5.